# Homology Modeling Identifies C-Terminal Residues that Contribute to the $Ca^{2+}$ Sensitivity of a $BK_{Ca}$ Channel

Jian-Zhong Sheng,* Aalim Weljie,† Lusia Sy,* Shizhang Ling,* Hans J. Vogel,† and Andrew P. Braun*
Departments of *Pharmacology and Therapeutics and †Biological Sciences, University of Calgary, Calgary, Alberta, Canada

ABSTRACT Activation of $BK_{Ca}$ channels by direct $Ca^{2+}$ binding and membrane depolarization occur via independent and additive molecular processes. The ''calcium bowl'' domain is critically involved in $Ca^{2+}$-dependent gating, and we have hypothesized that a sequence within this domain may resemble an EF hand motif. Using a homology modeling strategy, it was observed that a single $Ca^{2+}$ ion may be coordinated by the oxygen-containing side chains of residues within the calcium bowl (i.e., $^{912}$ELVNDTNVQFLD$^{923}$). To examine these predictions directly, alanine-substituted $BK_{Ca}$ channel mutants were expressed in HEK 293 cells and the voltage and $Ca^{2+}$ dependence of macroscopic currents were examined in inside-out membrane patches. Over the range of 1–10 $\mu$M free $Ca^{2+}$, single point mutations (i.e., E912A and D923A) produced rightward shifts in the steady-state conductance-voltage relations, whereas the mutants N918A or Q920A had no effect on $Ca^{2+}$-dependent gating. The double mutant E912A/D923A displayed a synergistic shift in $Ca^{2+}$-sensitive gating, as well as altered kinetics of current activation/deactivation. In the presence of 1, 10, and 80 mM cytosolic $Mg^{2+}$, this double mutation significantly reduced the $Ca^{2+}$-induced free energy change associated with channel activation. Finally, mutations that altered sensitivity of the holo-channel to $Ca^{2+}$ also reduced direct $^{45}$Ca binding to the calcium bowl domain expressed as a bacterial fusion protein. These findings, along with other recent data, are considered in the context of the calcium bowl's high affinity $Ca^{2+}$ sensor and the known properties of EF hands.

## INTRODUCTION

The large conductance, calcium-activated potassium channel ($BK_{Ca}$ channel) contributes to stimulus-induced changes in membrane potential in neurons, smooth muscle, and many secretory cells through its ability to open in response to membrane depolarization and elevated cytosolic free calcium in an additive fashion. The predicted membrane topology of the pore-forming $BK_{Ca}$ $\alpha$-subunit closely resembles those of voltage-gated $K^+$ channel subunits (e.g., Kv1-4 family members), with the added features of an extracellular N-terminus and long intracellular C-terminal tail. Initial efforts by Salkoff and co-workers to unravel the molecular properties underlying the $BK_{Ca}$ channel's calcium sensitivity have shown that a series of C-terminal Asp acid residues, dubbed the ''calcium bowl'', appears to be critically involved (31,32). Subsequent studies taking advantage of mutational analyses have identified two additional regions within the large C-terminus of the $BK_{Ca}$ $\alpha$-subunit that selectively influence the calcium sensitivity of channel activation (3,38). Thus, neutralization/elimination of acidic residues in the calcium bowl, together with substitutions at positions D362 and D367 (e.g., D362A/D367A) (38) or M513 (e.g., M513I) (3) in the C-terminus have been shown to abolish the calcium-dependent activation of $BK_{Ca}$ channels at free $Ca^{2+}$ concentrations $\leq$100 $\mu$M. An additional low-affinity divalent metal binding site, located within the channel's ''RCK domain'' (34,38), further contributes to activation at concentrations of divalent cation $>$0.1 mM. Very recently, Lingle and co-workers (39) have demonstrated that the regulation of $BK_{Ca}$ channel gating by each of these three sites displays a distinct activation profile in response to a series of divalent metals (e.g., $Ca^{2+}$, $Sr^{2+}$, $Cd^{2+}$, $Mn^{2+}$, $Co^{2+}$, and $Ni^{2+}$), thereby strengthening the argument that the $BK_{Ca}$ $\alpha$-subunit contains three physically separate divalent metal binding sites. Such activation profiles may further suggest differences in the structural features underlying each of these sites.

Using a $^{45}$Ca overlay assay, it has been demonstrated that a ~230 amino acid fragment of the $BK_{Ca}$ $\alpha$-subunit from either mouse brain (2,5) or *Drosophila* (4) directly binds radioactive $^{45}$Ca and that this binding is disrupted by replacement of acidic residues within the calcium bowl segment. Such observations are consistent with, but do not prove, the hypothesis that this domain directly contributes to high-affinity $Ca^{2+}$ ion binding, rather than acting as a ''transduction module'' that transfers the energy of $Ca^{2+}$ binding at a distinct site to the gating machinery in the channel core. Although it is now evident that the calcium bowl functionally contributes to $BK_{Ca}$ channel activation by physiologic levels of cytosolic $Ca^{2+}$, the structural features of this domain that underlie $Ca^{2+}$ binding remain undefined. Having noted earlier that the positions of oxygen-containing residues within this region align similarly with those in a canonical EF hand motif (5), we have utilized a homology modeling strategy to generate a predicted structure of this domain that describes the coordination of a single $Ca^{2+}$ ion

*Submitted March 27, 2005, and accepted for publication July 27, 2005.*

Address reprint requests to Andrew P. Braun, Dept. of Pharmacology and Therapeutics, Faculty of Medicine, University of Calgary, 3330 Hospital Dr., NW, Calgary, Alberta T2N 4N1, Canada. Tel.: 403-220-8861; Fax: 403-270-2211; E-mail: abraun@ucalgary.ca.



0006-3495/05/11/3079/14 $2.00

doi: 10.1529/biophysj.105.063610

by acidic amino acids within a putative loop structure. After experimental examination of these predictions, our results show that alanine substitution of acidic residues, corresponding to the X and −Z binding ligands within a canonical EF hand, decreased the calcium sensitivity of $BK_{Ca}$ channel activation in a synergistic manner by micromolar concentrations of $Ca^{2+}$. These same substitutions also significantly decreased direct $^{45}Ca$ binding to this domain expressed as a fusion protein in bacteria. In light of these data and other recent reports, we consider the possibility that an EF hand-like motif may contribute to the properties of the high-affinity $Ca^{2+}$ sensor located within the calcium bowl region of the $BK_{Ca}$ $\alpha$-subunit.

## MATERIALS AND METHODS

The cDNA constructs encoding the mouse brain *mSlo* $\alpha$-subunit (26) and green fluorescent protein, along with procedures for site-directed mutagenesis and transient transfection of HEK 293 cells have been recently described (5). All mutations were directly confirmed by either single or double-stranded cDNA sequencing. Note that the amino acid numbering of our *mSlo* clone, which contains a C-terminal splicing insert (15), is slightly different than that used by other investigators for another mouse brain *mSlo* clone without the insert (6). As a consequence, identical residues in the calcium bowl that have been mutated by both us and other investigators (e.g., Cox and colleagues) are denoted by higher numbering in our study. To assist the reader, we have indicated identical amino acids using both numbering schemes in the text, where appropriate.

### Electrophysiological measurements

Macroscopic currents were recorded at 35 ± 0.5°C from excised inside-out membrane patches of HEK 293 cells transiently transfected with either wild-type or mutant $BK_{Ca}$ channels, as previously described (5). For mutant channels with reduced calcium sensitivity (e.g., E912A/D923A), a more positive range of voltage-clamp steps was often used to produce maximal open probability of the macroscopic currents. Micropipettes were filled with a solution containing (in millimolar): 5 KCl, 125 KOH, 1 $MgCl_2$, 1 $CaCl_2$, 10 HEPES, pH adjusted to 7.3 with methanesulfonic acid and had tip resistances of 1.5–3.5 MΩ. Voltage clamp error associated with series resistance was compensated to a level of 80% using the electronic circuitry of the Axopatch 200B amplifier. The bath solution contained (in millimolar): 5 KCl, 125 KOH, 1 $MgCl_2$, 2 EGTA or HEDTA, 10 HEPES; the pH was adjusted to ~7.25 with methanesulfonic acid. The level of free calcium in each bath solution was then independently confirmed using a calcium electrode (Orion model 93-20) with calibration standards (World Precision Instruments, Sarasota, FL) ranging from pCa 8 to 2.

For recordings in the presence of elevated $MgCl_2$, the bath solution was modified to account for changes in osmolality with increasing concentrations of $MgCl_2$. The 1-mM $MgCl_2$ solution contained 50 mM KOH and 80 mM *N*-methyl D-glucamine (NMDG), the 10 mM $MgCl_2$ solution contained 50 mM KOH and 70 mM NMDG, and the 80 mM $MgCl_2$ solution contained only 50 mM KOH. The desired level of free calcium in each solution was obtained by addition of either 2 mM EGTA or 100 $\mu$M $CaCl_2$, and pH was adjusted to 7.2 with methanesulfonic acid. The recording pipette was filled with the 1-mM $MgCl_2$ bath solution (see above) that was supplemented with 100 $\mu$M $CaCl_2$. Although intracellular NMDG has been previously reported to produce a modest block of $BK_{Ca}$ channel current (21), the effect should be minimal at the tail current potentials used in our experiments (i.e., −80 and −120 mV). Furthermore, any amount of block would be expected to be uniform for both the wild-type and mutant channels at these tail potentials and should therefore not affect either the calculated half-maximal voltages of activation or the comparisons made between the channel types at 1 and 10 mM free $Mg^{2+}$ concentrations.

### Computer modeling of the $BK_{Ca}$ channel C-terminal domain

The structural coordinates corresponding to a 36-amino-acid sequence spanning the third EF hand (EFIII) of human calmodulin were extracted from the Protein Data Bank file 1CLL.pdb and used as a template for an equivalent stretch of residues from the C-terminus of the $BK_{Ca}$ channel $\alpha$-subunit. Model building was performed using the Homology Modeling module of the software package Insight II (Accelrys, San Diego, CA), and the step-by-step modeling procedure closely followed that recently utilized to generate an experimentally valid model of the calmodulin-like domain of a calcium-sensitive protein kinase from soybean (36). Provided in this study is a detailed description of the structural and energetic constraints invoked as the modeling procedure progressed toward the determination of a final predicted structure (36). The procedure consisted of iterative rounds of molecular dynamics and energy minimization differentially applied to regions of the calcium bowl considered to be either ''variable'' or ''conserved''. The parameters chosen for modeling the selected $BK_{Ca}$ channel C-terminal sequence were sufficiently stringent to indicate if some aspect of the modeled sequence was grossly inadequate (e.g., too much steric interference by large residues, the length of the sequence was too long/short to act as an EF hand, etc.) and would prevent the generation of a plausible model. In addition, as we reasoned a priori that an EF hand-like motif may exist within the calcium bowl, the regions postulated to be part of the EF hand motif were treated as ''conserved'' during the modeling process and the remainder as ''variable''. Charge effects were taken into account by incorporating a single $Ca^{2+}$ ion in the calculations used to generate the final predicted structure. The software program MolMol was used to create the final images shown in Fig. 2.

### Direct $^{45}Ca$ binding to bacterial fusion proteins

A region of 148 amino acids (i.e., $^{861}$NSPV.. to ..CRVA$^{1009}$) that included the entire calcium bowl domain was isolated as a cDNA fragment by polymerase chain reaction from the C-terminus of the wild-type $BK_{Ca}$ $\alpha$-subunit, and mutant $\alpha$-subunits containing engineered amino acid substitutions. Individual cDNA fragments were subcloned into the bacterial expression vector pET15b using *Nde*I and *Bam*HI restriction sites, which resulted in the addition of a 21-amino-acid segment containing a 6× His affinity purification tag to the N-terminus of the $BK_{Ca}$ channel fragment. Expression of His-tagged fusion proteins in the BL21 (DE3) strain of *E. coli* (200-ml cultures) was induced for ~3 h at 35°C after addition of 0.1 mM IPTG. Bacteria were collected by centrifugation at 1000 × g for 10 min at 4°C and then resuspended in buffer A (i.e., 50 mM $NaH_2PO_4$, 300 mM NaCl, pH 7.0) containing 1 mg/ml lysozyme. Bacteria were lysed by freeze/thaw, sonicated for 1 min, and the $BK_{Ca}$ $\alpha$-subunit fusion proteins were extracted from the insoluble material by a 1-h incubation at room temperature in buffer B (10 mM Tris HCl, pH 8, 100 mM $NaH_2PO_4$, 6 M urea, and 10 mM imidazole). After incubation of solubilized fusion proteins with 1–2 ml of $Ni^{2+}$-NT agarose beads (Qiagen, Valencia, CA) (1 h, 4°C), the resin was washed three times with 20 mM Tris HCl, pH 8, 500 mM NaCl, 6 M urea, and 40 mM imidazole. Bound proteins were then eluted with buffer containing 50 mM $NaH_2PO_4$, 300 mM NaCl, and 250 mM imidazole, pH 8. After overnight dialysis to remove excess salts, equal amounts of purified fusion proteins were mixed with Laemmli sample buffer, resolved by SDS-PAGE, and then electrotransferred to 0.2 $\mu$m nitrocellulose membrane. Direct $^{45}Ca$ binding to proteins transferred to nitrocellulose membrane was performed essentially as previously described (5). Briefly, nitrocellulose membranes were washed four times in buffer (60 mM KCl, 5 mM $MgCl_2$, 10 mM imidazole HCl, pH 6.8) and then incubated for 10 min at room temperature with the same buffer containing ~10 $\mu$M $^{45}Ca$.

Membranes were washed for 5 min in 200 ml of 50% ethanol to remove unbound $^{45}Ca$ and then dried. $^{45}Ca$ binding to individual fusion proteins was quantified using a PhosphorImager (Molecular Dynamics, Piscataway, NJ) and membranes were then stained with 0.1% (w/v) amido black. The amount of fusion protein on the membrane corresponding to each $^{45}Ca$-labeled band was quantified using Quantity One image analysis software (Bio-Rad Laboratories, Hercules, CA).

## Data analysis

Pairs of current-voltage relations were recorded at each concentration of free $Ca^{2+}$, and the current families were then averaged for subsequent analysis. Normalized conductance-voltage (G-V) relations were calculated from tail current amplitudes measured 0.25 ms following the step to the tail potential. All G-V relations were fit with single Boltzmann functions, according to the equation:

$$G / Gmax = 1 / (1 + e^{zF(V1/2-Vm)/RT}), \qquad \text{(Eq.1)}$$

where $Vm$ is the experimental test potential (in volts), $V_{1/2}$ is the half-maximal voltage of activation (in volts), defined as the membrane potential at which 50% of the channels are open, $z$ is the valence of the permeable ion, and $F/RT = 37.67/V$ at 35°C.

The time constants ($\tau$) of deactivation were derived from single exponential fits of macroscopic tail currents recorded at potentials ranging from −100 to +50 mV, in response to activating voltage-clamp steps to either 160 mV (4 $\mu$M $Ca^{2+}$) or 80 mV (10–400 $\mu$M $Ca^{2+}$). Exponential fits were performed over a period of 4–5 ms, beginning 0.25–0.3 ms after the step to the tail current potential. Similarly, time constants of activation were determined from single exponential fits to currents over a period of 7–10 ms, beginning 0.25 ms after the start of the voltage-clamp step to the indicated membrane potentials.

Values for wild-type and mutant $BK_{Ca}$ channels were examined statistically using either a one-way analysis of variance and appropriate post-hoc test or an unpaired Student's $t$-test; differences between values were considered to be statistically significant at level of $p < 0.05$.

# RESULTS

## Sequence alignment of the calcium bowl region with an EF hand motif raises the possibility of structural similarity

We have previously reported that a series of residues contained within the calcium bowl region of the $BK_{Ca}$ channel $\alpha$-subunit displays characteristics reminiscent of the $Ca^{2+}$-binding properties of an EF hand structure (5). As noted in Fig. 1, the amino acid sequence adjacent to a series of aspartic acids contains a number of residues with oxygen-containing side chains in positions that correspond to the $Ca^{2+}$ coordinating ligands present in the divalent ion binding loops of both classic and variant EF hand structures (19). In this study, we have utilized a homology modeling strategy to examine more objectively whether this region associated with the calcium bowl domain may be predicted to resemble a bona fide EF hand and if additional residues contributing to the calcium sensitivity of channel gating via this domain could be thus identified.

Fig. 2 *A* shows the solved structure of the third EF hand of human calmodulin in its $Ca^{2+}$-bound form (7). The helix-loop-helix arrangement of the main-chain carbon backbone

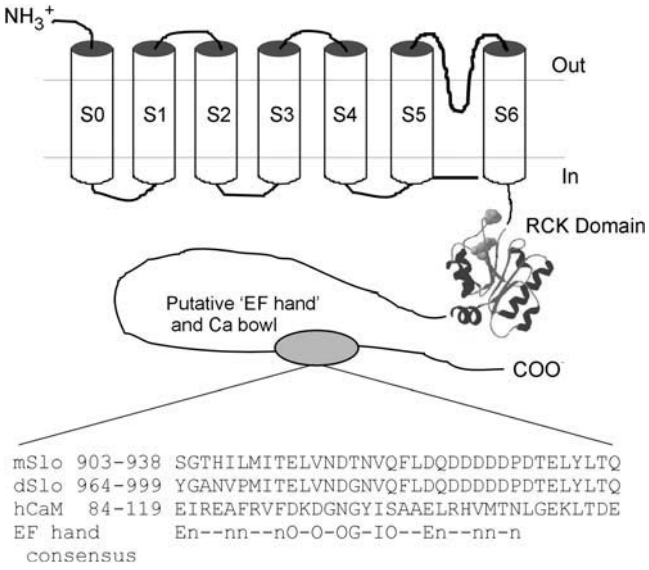


FIGURE 1 A region associated with the calcium bowl domain of the $BK_{Ca}$ channel $\alpha$-subunit displays similarity to an EF hand motif. The cartoon of the $BK_{Ca}$ $\alpha$-subunit shows the location of the C-terminal calcium bowl relative to the channel's transmembrane segments, the pore loop positioned between S5 and S6 and the low-affinity $Mg^{2+}/Ca^{2+}$-binding site associated with the channel's RCK domain (17). Below the cartoon is a comparison of the amino acid sequences of the calcium bowl from mouse (*mSlo*) and *Drosophila* (*dSlo*) $BK_{Ca}$ channel $\alpha$-subunits (1,26) with that of the third EF hand of human calmodulin (*hCaM*) and an EF hand consensus motif (24). ''O'' and ''n'' denote oxygen-containing (i.e., D, E, N, Q, S, T) and nonpolar residues, respectively.

is evident, along with the single $Ca^{2+}$ ion coordinated by side-chain oxygen atoms near the center of the loop. For purposes of clarity, only the residues that serve as direct $Ca^{2+}$-coordinating ligands are displayed. Using standard homology modeling techniques, this EF hand structure was utilized as a template to model an analogous series of 36 amino acids within the calcium bowl region of the $BK_{Ca}$ channel $\alpha$-subunit (refer to sequence alignment in Fig. 1). The $\alpha$-carbon backbone of the predicted structure (Fig. 2 *B*) displays a helix-loop-helix pattern, with a less well-ordered region beyond Asp-929 (the last side-chain group displayed in the C-terminal region). Of the six residues with oxygen-containing side chains in the sequence alignment that may act as potential $Ca^{2+}$-coordinating ligands (i.e., Glu-912, Asn-915, Asp-916, Asn-918, Gln-920, and Asp-923) (refer to Fig. 1), the side chains of only Glu-912, Asp-916, and Asp-923 appear to be oriented toward the center of the predicted loop structure, such that they may physically coordinate a single $Ca^{2+}$ ion (Fig. 2 *B*). The predicted distances between these side-chain oxygen atoms and the bound $Ca^{2+}$ ion range from 2.2 to 3 Å, which are consistent with those seen in the loop structures of $4Ca^{2+}$-bound form of calmodulin (13). As the side chains of the three remaining oxygen-containing residues (i.e., Asn-915, Asn-918, and Gln-920) are positioned away from the center of the loop, it may be anticipated that they would not contribute to $Ca^{2+}$ ion

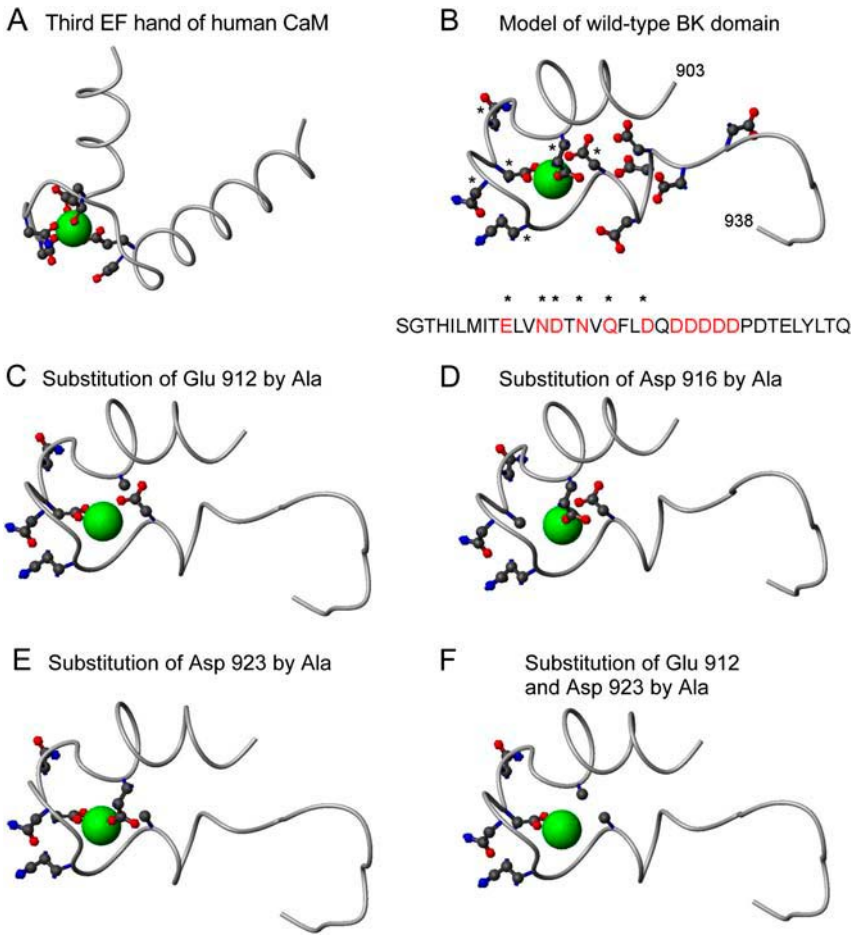


FIGURE 2 Structural models of the calcium bowl region generated by homology modeling using atomic coordinates from the $Ca^{2+}$-bound form of human calmodulin (7). In panel *A*, the backbone carbon structure of the third EF hand of calmodulin is shown in a ribbon diagram; the side chains of the six $Ca^{2+}$ coordinating amino acids are shown in ball-and-stick format, with oxygen, nitrogen, and carbon atoms represented by red, blue, and black balls, respectively. Note that the same color-coding scheme is also used for these atoms in panels *B–F*. Hydrogen atoms have been omitted for clarity. The position of a single bound $Ca^{2+}$ ion within the EF hand structure is represented by the green sphere. Panel *B* shows a molecular model generated using a 36-amino-acid sequence of a mouse brain $BK_{Ca}$ $\alpha$-subunit (26) that contains potential $Ca^{2+}$ coordinating residues with homology to those found within an EF hand (refer to Fig. 1). The oxygen-containing side chains of these amino acids (i.e., E912, N915, D916, N918, Q920, and D923) are denoted by asterisks both in the model and the single letter, primary sequence shown below. Also displayed are the oxygen-containing side chains of the five Asp residues within the calcium bowl that have been previously reported to influence the $Ca^{2+}$ sensitivity of $BK_{Ca}$ channel activation (2,4,31,32,38). Note that all of the residues with oxygen-containing side chains shown in the model are indicated by red lettering in the primary sequence beneath. Shown in panels *C–F* are models of $BK_{Ca}$ $\alpha$-subunit mutants generated after alanine replacement of one or more acidic residues in the channel's primary sequence. For clarity, the side chains of the five Asp residues depicted in panel *B* have been omitted. The green sphere within each predicted $BK_{Ca}$ channel structure represents a bound $Ca^{2+}$ ion, the position of which has been assigned by the modeling software in accordance with energetic constraints.

binding. In addition, the model shows the side chains of the five adjacent Asp residues, which appear to form an $\alpha$-helical turn. Previously, it has been demonstrated that replacement/deletion of some or all of this Asp-rich sequence dramatically reduces the $Ca^{2+}$ sensitivity of $BK_{Ca}$ channel gating (2,3,31,32,38). In our model, several of these side chains are oriented toward the bound $Ca^{2+}$ ion, suggesting that they may influence $Ca^{2+}$ binding. Bao and colleagues have recently shown that a stretch of amino acids within the calcium bowl encompassing this Asp-rich region (i.e., QDDDDDPDTELY) may be modeled as a $Ca^{2+}$-binding structure when the 12-residue loop region of the first EF hand of carp parvalbumin (i.e., QDKSGFIEEDEL) is used as a structural template (2).

Given the predicted roles of Glu-912, Asp-916, and Asp-923 as $Ca^{2+}$-binding ligands in the wild-type $BK_{Ca}$ $\alpha$-subunit, we also generated homology models containing single or double alanine substitutions of these predicted $Ca^{2+}$-coordinating residues by repeating the modeling procedure with the modified primary amino acid sequences (Fig. 2, *C–F*). We did not observe significant changes in the main-chain carbon backbone structure of these mutant models, indicating that these individual substitutions did not energetically destabilize the modeling routine.

## Replacement of predicted $Ca^{2+}$-binding residues decreases the calcium sensitivity of steady-state gating and the kinetics of current activation/deactivation

To test experimentally the predicted importance of the $Ca^{2+}$-binding residues identified by our modeling efforts on the calcium sensitivity of $BK_{Ca}$ channel gating, we carried out individual alanine substitution of the six oxygen-containing residues noted above and transiently expressed the mutant $BK_{Ca}$ channel $\alpha$-subunits in HEK 293 cells. Several of the mutations examined in our study have also been recently described by Bao and colleagues using another mouse brain *mSlo* clone (2) that lacks a C-terminal splice insert (15). To allow the reader to follow more easily the two data sets, we have included their numbering scheme (in parentheses) along with ours when referring to the same amino acids.

Macroscopic current activities of both wild-type and mutant channels were recorded in excised inside-out membrane patches in the absence and presence of free cytosolic $Ca^{2+}$. Fig. 3 shows representative tracings of current families recorded over a broad range of membrane voltage and cytosolic [$Ca^{2+}$]s. Compared to the wild-type channel, currents arising from the E912(884)A and D923(895)A mutants displayed slower activation and faster deactivation kinetics at free [$Ca^{2+}$]s ranging from 1 to 100 $\mu$M, and these characteristics were more pronounced in the E912A/D923A double mutant. However, at higher $Ca^{2+}$ concentrations (i.e., 400 and 1000 $\mu$M), kinetic changes observed in either the single or double mutant channels were no longer evident. In contrast to these observations, alanine substitution of either D916(888) (Fig. 3), N918(890), or Q920(892) (data not shown) did not produce obvious changes in the calcium-dependent gating of these channels. Unfortunately, the N915(887)A mutant did not express well enough in our hands for reliable measurements; however, this same mutation appeared to have no effect on the calcium sensitivity of another mouse brain $BK_{Ca}$ channel expressed in *Xenopus* oocytes (2).

Plots of conductance-voltage (G-V) relations derived from measurements of the tail current amplitudes for the wild-type and the five mutant $BK_{Ca}$ channels described above were fit with single Boltzmann functions, yielding values for the half-maximal voltages of activation ($V_{1/2}$ value) and the apparent equivalent gating charge ($z$). A summary of these values (means ± SE) are listed in Table 1 and a plot of the absolute $V_{1/2}$ values is shown in Fig. 4 *A*. Due to the modest

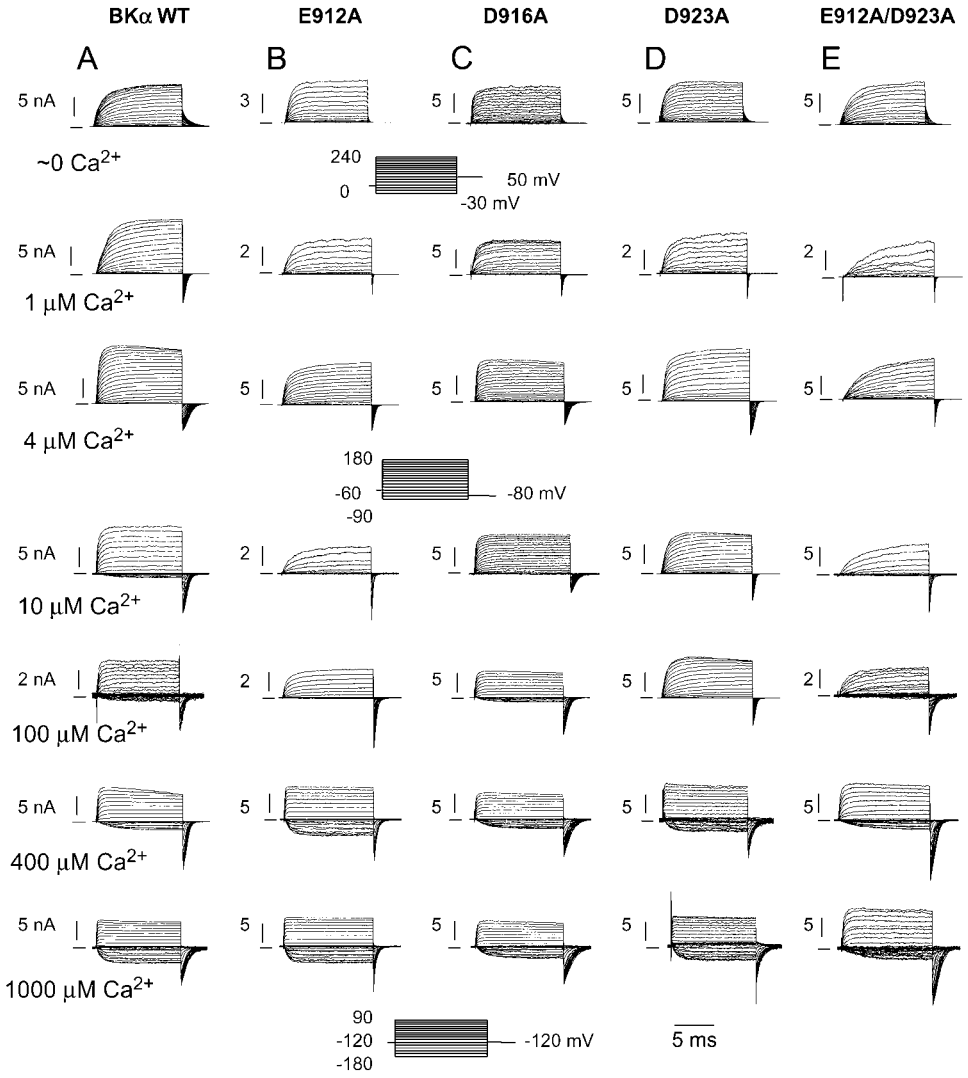


FIGURE 3 Macroscopic currents recorded from wild-type or mutant $BK_{Ca}$ channels in excised inside-out membrane patches. cDNAs encoding wild-type (column *A*), the E912(884)A mutant (column *B*), the D916(888)A mutant (column *C*), the D923(895)A mutant (column *D*), or the E912A/D923A double mutant (column *E*) forms of the $BK_{Ca}$ channel $\alpha$-subunit were transiently expressed in HEK 293 cells as described in Materials and Methods. Current families were recorded in response to increasing concentrations of cytoplasmic $Ca^{2+}$, which are denoted on the left-hand side. The horizontal dash preceding each family of current tracings indicates the zero current level. For zero $Ca^{2+}$ conditions (i.e., 2 mM EGTA alone), voltage-clamp steps from −30 to 240 mV, and were given from a holding potential of 0 mV. For 1 and 4 $\mu$M free $Ca^{2+}$ concentrations, steps ranged from −90 to 180 mV and the holding potential was −60 mV. For $Ca^{2+}$ concentrations between 10 and 1000 $\mu$M, voltage steps ranged from −180 to 90 mV, using a holding potential of −120 mV. For all three protocols, the increment between consecutive voltage-clamp steps was 10 mV. The voltage-clamp protocols used experimentally are depicted beneath their respective rows of current tracings. Current records are shown as the average of two independent current-voltage families recorded sequentially at each free [$Ca^{2+}$]. The number adjacent to the vertical scale bar in each panel indicates current amplitude in nanoamperes. The timescale indicated by the horizontal bar at the bottom of the figure applies to all current tracings. Note that for a given channel type, displayed currents were recorded from the same membrane patch over the range of indicated free [$Ca^{2+}$]s; exceptions to this are the current tracings shown for the wild-type and E912A/D923A double mutant channels at 100 $\mu$M free $Ca^{2+}$, which were each recorded from different membrane patches. In a few cases, the vertical scaling of current tracings was adjusted to maintain a uniform size for displayed current families; such adjustments reflect differences in current amplitudes observed for wild-type and mutant channels using a particular voltage-clamp protocol and free [$Ca^{2+}$].

**TABLE 1 Parameters derived from Boltzmann fits to wild-type and mutant $BK_{Ca}$ channel G-V curves**

| [Calcium]* | BK channel description | $V_{1/2}$-value (mV) | $z$-value | $n$ |
|---|---|---|---|---|
| 5 nM | Wild-type | 163.4 ± 2.3 | 1.19 ± 0.04 | 13 |
| | E912A | 192.4 ± 4.0 | 1.14 ± 0.04 | 5 |
| | D916A | 162.3 ± 2.2 | 1.29 ± 0.10 | 4 |
| | N918A | 160.8 ± 3.9 | 1.19 ± 0.07 | 6 |
| | Q920A | 163.3 ± 2.2 | 1.18 ± 0.07 | 6 |
| | D923A | 158.7 ± 7.2 | 1.17 ± 0.08 | 9 |
| | E912A/D923A | 187.4 ± 2.2 | 1.12 ± 0.04 | 14 |
| 1 $\mu$M | Wild-type | 129.5 ± 6.6 | 1.16 ± 0.04 | 8 |
| | E912A | 183.0 ± 4.5 | 1.12 ± 0.04 | 9 |
| | D916A | 115.7 ± 5.9 | 1.41 ± 0.10 | 5 |
| | N918A | 123.2 ± 5.4 | 1.05 ± 0.09 | 5 |
| | Q920A | 118.7 ± 3.6 | 1.07 ± 0.05 | 6 |
| | D923A | 156.3 ± 4.6 | 1.26 ± 0.05 | 10 |
| | E912A/D923A | 189.8 ± 3.3 | 1.16 ± 0.03 | 8 |
| 4 $\mu$M | Wild-type | 66.7 ± 8.7 | 1.18 ± 0.06 | 7 |
| | E912A | 123.7 ± 5.3 | 1.04 ± 0.05 | 10 |
| | D916A | 75.1 ± 2.6 | 1.19 ± 0.09 | 5 |
| | N918A | 61.7 ± 8.2 | 1.10 ± 0.09 | 6 |
| | Q920A | 61.4 ± 5.7 | 1.06 ± 0.05 | 7 |
| | D923A | 116.5 ± 7.1 | 1.19 ± 0.04 | 10 |
| | E912A/D923A | 161.2 ± 5.2 | 1.18 ± 0.05 | 13 |
| 10 $\mu$M | Wild-type | −3.3 ± 6.3 | 1.25 ± 0.07 | 5 |
| | E912A | 34.8 ± 9.6 | 1.21 ± 0.09 | 8 |
| | D916A | 16.3 ± 2.6 | 1.21 ± 0.06 | 4 |
| | N918A | −4.3 ± 4.2 | 1.39 ± 0.05 | 5 |
| | Q920A | −0.9 ± 2.4 | 1.12 ± 0.07 | 7 |
| | D923A | 43.7 ± 7.4 | 1.34 ± 0.08 | 8 |
| | E912A/D923A | 125.0 ± 7.0 | 1.20 ± 0.03 | 13 |
| 100 $\mu$M | Wild-type | −33.8 ± 4.5 | 1.28 ± 0.04 | 9 |
| | E912A | −10.1 ± 3.4 | 1.31 ± 0.06 | 7 |
| | D916A | −32.1 ± 2.8 | 1.29 ± 0.07 | 5 |
| | N918A | −41.7 ± 2.1 | 1.15 ± 0.05 | 5 |
| | Q920A | −39.2 ± 1.9 | 1.30 ± 0.08 | 7 |
| | D923A | −3.5 ± 6.8 | 1.37 ± 0.11 | 5 |
| | E912A/D923A | 36.9 ± 3.1 | 1.24 ± 0.07 | 13 |
| 400 $\mu$M | Wild-type | −41.4 ± 3.8 | 1.35 ± 0.09 | 7 |
| | E912A | −48.4 ± 3.7 | 1.36 ± 0.10 | 4 |
| | D916A | −51.2 ± 1.6 | 1.40 ± 0.10 | 4 |
| | D923A | −53.6 ± 4.6 | 1.35 ± 0.09 | 6 |
| | E912A/D923A | 18.3 ± 6.7 | 1.33 ± 0.10 | 4 |
| 1000 $\mu$M | Wild-type | −53.0 ± 3.9 | 1.41 ± 0.08 | 7 |
| | E912A | −53.8 ± 2.9 | 1.34 ± 0.03 | 4 |
| | D916A | −61.9 ± 2.1 | 1.35 ± 0.10 | 4 |
| | N918A | −47.3 ± 2.5 | 1.13 ± 0.04 | 5 |
| | Q920A | −45.3 ± 2.2 | 1.30 ± 0.13 | 5 |
| | D923A | −57.9 ± 7.5 | 1.32 ± 0.05 | 4 |
| | E912A/D923A | −41.7 ± 5.2 | 1.26 ± 0.05 | 5 |

Data are presented as means ± SE; $n$ indicates the number of excised membrane patches used experimentally for each condition.

*Stated parameters were calculated according to the following Boltzmann function: $G / Gmax = 1 / (1 + e^{zF(V1/2-Vm)/RT})$, where $V_{1/2}$ is the half-maximal voltage of activation, $Vm$ is the membrane potential, $z$ is the apparent gating valence, $F$ is Faraday's constant (96,485 C/mol), $R$ is the gas constant (8.3145 VC/mol K), and $T$ is the experimental temperature in Kelvin (308 K).

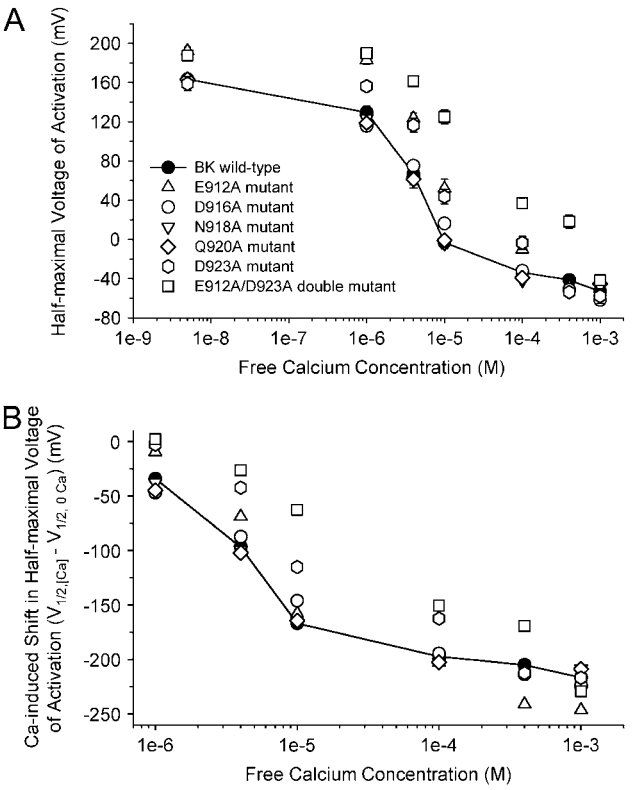


FIGURE 4 Mutations predicted to reduce $Ca^{2+}$ sensitivity alter the half-maximal voltages of $BK_{Ca}$ current activation ($V_{1/2}$ values) in the presence of cytoplasmic free $Ca^{2+}$. In panel *A*, $V_{1/2}$ values for both wild-type and mutant channels were derived from single Boltzmann functions fit to normalized conductance-voltage plots calculated from individual current recordings at each [$Ca^{2+}$]. In panel *B*, $V_{1/2}$ values for each channel type have been ''normalized'' by calculating the difference between the average $V_{1/2}$ value obtained in nominally free $Ca^{2+}$ (*A*) and the average $V_{1/2}$ values obtained in the presence of increasing concentrations of cytosolic $Ca^{2+}$ (e.g., $V_{1/2,\ 1\ \mu M\ Ca} - V_{1/2,\ 0\ Ca}$). Data are presented as means ± SE. The number of membrane patches used to calculate the mean data points at the indicated concentrations of $Ca^{2+}$ for the wild-type and mutant channels varied as follows: wild-type, five to eight patches; E912A, four to 10 patches; D916A, four to five patches; D923A, four to 10 patches; E912A/D923A double mutant, four to 12 patches.

rightward shifts in activation observed for the E912A and E912A/D923A mutant $BK_{Ca}$ channels in the absence of $Ca^{2+}$ (i.e., 2 mM EGTA alone), we have also expressed the calcium-dependent $V_{1/2}$ values relative to the 0 Ca value by calculating the differences between $V_{1/2}$ values in the presence of cytosolic $Ca^{2+}$ (i.e., 1–1000 $\mu$M) and that in the absence of $Ca^{2+}$ for each channel type (Fig. 4 *B*). Even when accounting for these modest offsets, it remains evident that the E912(884)A, D923(895)A, and E912A/D923A channel mutants display reduced calcium sensitivity (i.e., a decrease in the ability of increasing concentrations of cytosolic free $Ca^{2+}$ to evoke leftward shifts of G-V curves along the voltage axis) compared to the wild-type $BK_{Ca}$ channel.

Given that the activation and deactivation kinetics of macroscopic $BK_{Ca}$ channel currents are $Ca^{2+}$ dependent (10,12), the observed changes in the activation/deactivation

time courses of mutant $BK_{Ca}$ channel currents in the presence of cytosolic $Ca^{2+}$ (see Fig. 3) would be consistent with a reduced calcium sensitivity of these channels. To examine these phenomena in greater detail, the time courses of current activation and deactivation were quantified over broad ranges of membrane voltage and cytosolic [$Ca^{2+}$]. Fig. 5 *A* shows representative tracings of deactivating tail currents recorded from wild-type and mutant $BK_{Ca}$ channels in the presence of 4 and 100 $\mu$M concentrations of $Ca^{2+}$. Semilogarithmic plots of the time constants derived from single exponential fits of the rising and decaying phases of currents recorded in the presence of $Ca^{2+}$ concentrations ranging from 0 to 400 $\mu$M are shown in Fig. 5, *B* and *C*, respectively. In the presence of nominally free $Ca^{2+}$ (i.e., 2 mM EGTA), no major differences in either activation or deactivation time constants were observed between wild-type and mutant channels. However, over the range of 4–400 $\mu$M free $Ca^{2+}$, it is evident that the E912A and D923A mutants and E912A/D923A double mutant display slower activation kinetics compared to the wild-type channel. Similarly, these same

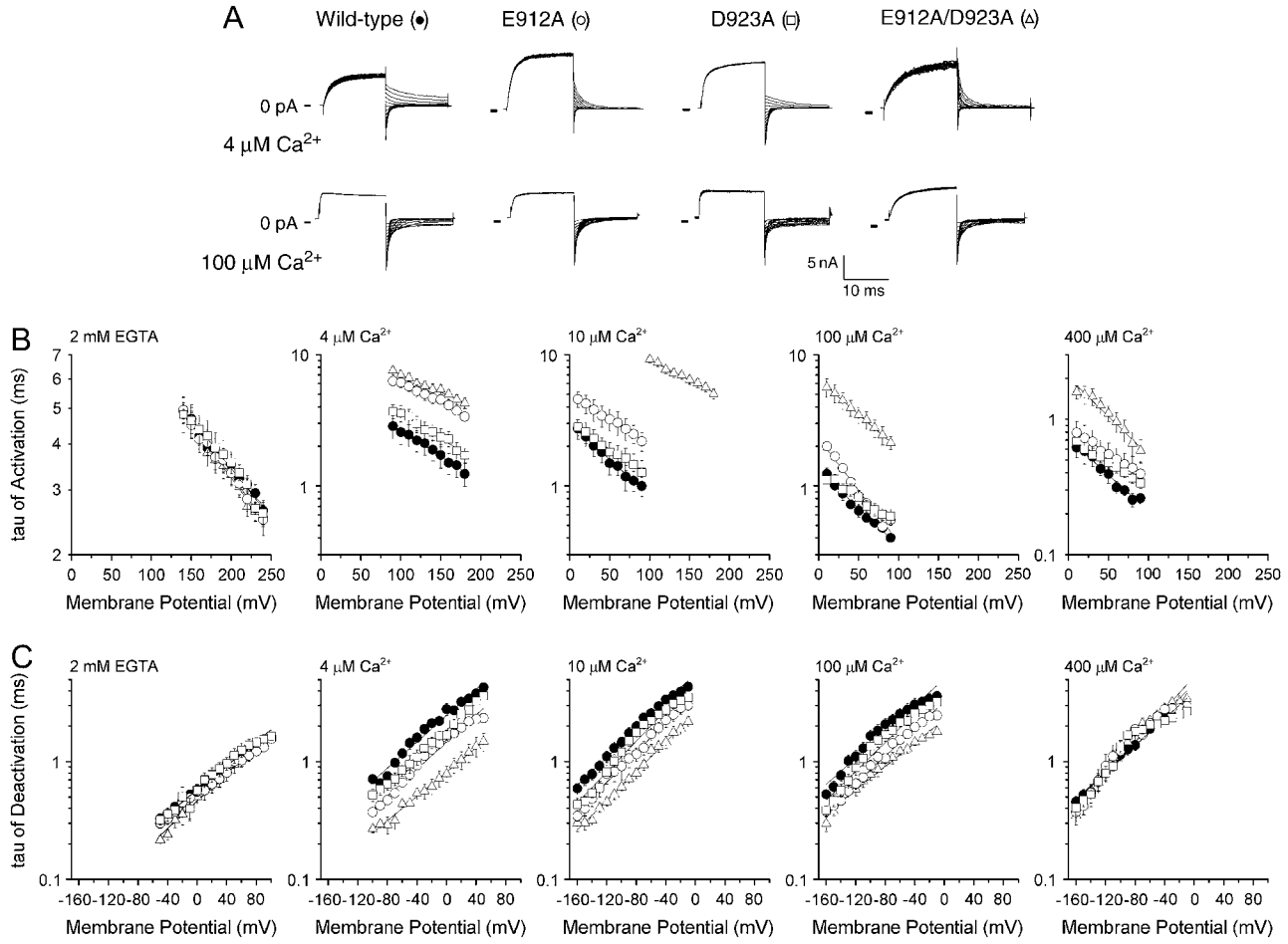


FIGURE 5 Mutations that decrease the $Ca^{2+}$ sensitivity of $BK_{Ca}$ channel gating also reduce the time constants of $BK_{Ca}$ current activation and deactivation. Panel *A* shows representative tail currents recorded from wild-type and mutant $BK_{Ca}$ channels at low and high $Ca^{2+}$ concentrations. In the presence of 4 $\mu$M $Ca^{2+}$, channels were first activated by a step pulse to +160 mV, and tail currents were then recorded at step potentials ranging from −100 to +50 mV, delivered in 10-mV increments. For recordings in the presence of 100 $\mu$M $Ca^{2+}$, a step pulse to +80 mV was used to activate channels, followed by step pulses to tail potentials ranging from −160 to −10 mV. The horizontal dash preceding each family of current recordings indicates the zero current level, and the vertical and horizontal scale bars at the bottom of the panel apply to all tracings. Panel *B* shows semilogarithmic plots of activation time constants versus membrane potential for macroscopic currents recorded from wild-type and individual mutant channels in the presence of 0, 4, 10, 100, and 400 $\mu$M free $Ca^{2+}$ concentrations. Semilogarithmic plots of the time constants of current deactivation versus membrane potential are displayed in panel *C* at the same free [$Ca^{2+}$]s. For panels *B* and *C*, symbols denoting the type of $BK_{Ca}$ channel are as follows: ●, wild-type; ○, E912(884)A mutant; □, D923(895)A; △, E912A/D923A double mutant. The activation time constants shown in panel *B* were derived from single exponential fits to the rising phases of current traces similar to those displayed in Fig. 3. The plotted time constants of current deactivation represent single exponential fits to the decay phases of tail current recordings similar to those shown in panel *A*. Values represent the means ± SE calculated from four to seven individual membrane patches for each channel type. Solid lines through the data represent nonlinear regression fits, according to the exponential equations: Activation Time Constant $= A \times e^{(-qFVm/RT)}$; Deactivation Time Constant $= A \times e^{(qFVm/RT)}$, where $A$ = the $\tau$-value at 0 mV, $q$ = slope of the function. $F$, $Vm$, $R$, and $T$ have the same values as defined earlier. For fits of the activation and deactivation time constants, the derived values of $q$ ranged from 0.26 to 0.38 and 0.30 to 0.41, respectively.

mutants also undergo somewhat faster current deactivation; however, this latter effect does not appear to be as robust as that observed for activation. This observation is thus consistent with recent data from Lingle and co-workers (39) suggesting that the calcium bowl domain may regulate $Ca^{2+}$-dependent activation, whereas the molecular process underlying current deactivation may be more dependent upon the second high-affinity $Ca^{2+}$ sensor associated with residues D362/D367 in the RCK domain.

## The effect of mutations on the high-affinity $Ca^{2+}$-binding sites can be isolated in the presence of elevated cytosolic $Mg^{2+}$

In addition to channel opening produced via the high affinity $Ca^{2+}$-binding sites, $BK_{Ca}$ gating may also be activated by a low-affinity, divalent cation binding site sensitive to millimolar concentrations of either $Mg^{2+}$ or $Ca^{2+}$ ions (35). Subsequently, this gating mechanism has been characterized more extensively (33,40), leading to the identification of the channel's ''RCK domain'' (17) as this lower affinity $Mg^{2+}$/$Ca^{2+}$-binding site (34). To examine the selective activation of $BK_{Ca}$ channel gating by low concentrations of cytosolic $Ca^{2+}$, we took advantage of a strategy in which $Ca^{2+}$ ion binding to the low-affinity site is effectively competed by high concentrations (e.g., $\geq$10 mM) of cytosolic free $Mg^{2+}$ ions (3,33,34). Upon saturation of this low-affinity binding site by $Mg^{2+}$ ions, cytosolic free $Ca^{2+}$ at concentrations up to 100 $\mu$M would be expected to influence channel gating by interacting primarily with the high-affinity sites associated with the calcium bowl and residues D362/D367 (38). Experimentally, families of currents were recorded both in the presence (e.g., 100 $\mu$M) and absence (e.g., 2 mM EGTA) of cytosolic $Ca^{2+}$, under conditions in which the free $Mg^{2+}$ concentration in the bath was increased from 1 to 10 to 80 mM. Normalized G-V relations were calculated from tail current measurements and $V_{1/2}$ values were derived from single Boltzmann fits of the data. The degree of leftward shift in the observed G-V relations (e.g., $\Delta V_{1/2}$) induced by 100 $\mu$M $Ca^{2+}$ was then utilized as an index of the calcium sensitivity of channel activation due to the high-affinity binding sites, as recently described (3). In the presence of 1 mM $Mg^{2+}$ (i.e., standard recording conditions), the observed $\Delta V_{1/2}$ value should reflect the actions of 100 $\mu$M $Ca^{2+}$ on both the high-affinity and low-affinity sites. In the presence of 80 mM $Mg^{2+}$, the degree of leftward shift induced by 100 $\mu$M $Ca^{2+}$ should be due primarily to actions at the high-affinity sites, as $Ca^{2+}$ binding to the low affinity is prevented by an 800-fold excess of $Mg^{2+}$. In the presence of 10 mM $Mg^{2+}$, one may expect an ''incomplete block'' of $Ca^{2+}$ binding at the low-affinity site by $Mg^{2+}$, given that these two cations bind with similar affinities (i.e., in the millimolar range), to this site (33,40).

Fig. 6, *A* and *B*, show conductance-voltage (G-V) relations for both the wild-type $BK_{Ca}$ channel and the E912A/D923A

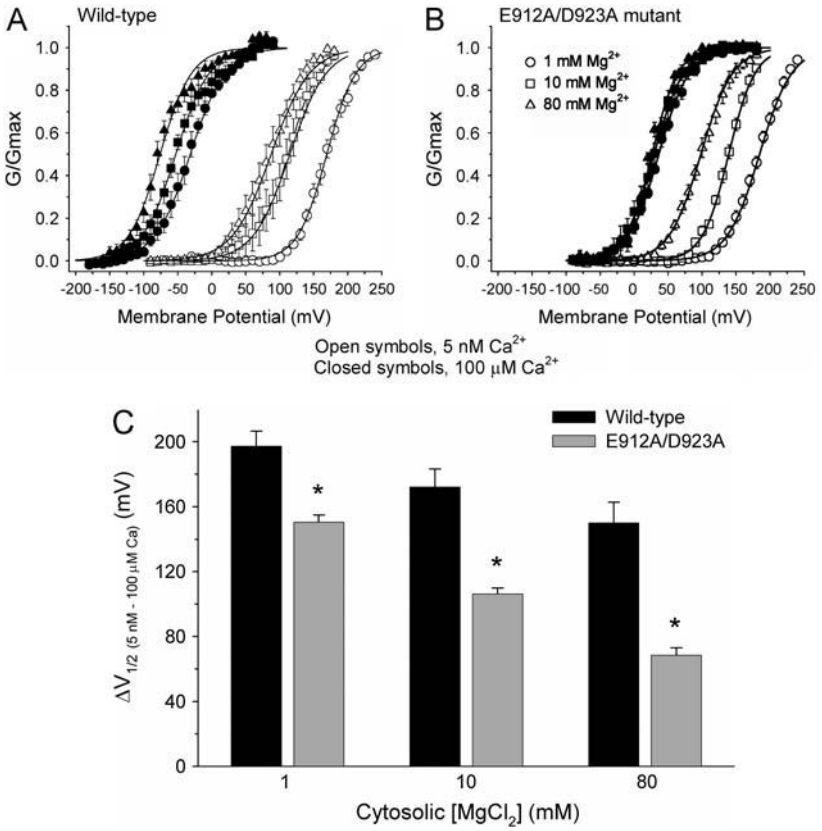


FIGURE 6 Elevated concentrations of cytosolic free $Mg^{2+}$ unmask the contribution of the high-affinity $Ca^{2+}$-binding sites to $BK_{Ca}$ channel gating. Current families were recorded from either wild-type $BK_{Ca}$ channels (*A*) or the E912A/D923A double mutant (*B*) in the presence of either nominally free (*open symbols*) or 100 $\mu$M (*solid symbols*) concentrations of $Ca^{2+}$, as described in Fig. 3. In addition to the absence or presence of free $Ca^{2+}$, cytosolic bath solutions contained free $Mg^{2+}$ at concentrations of 1, 10, or 80 mM. Normalized conductance-voltage relations (*G/Gmax* versus *Vm*) were calculated from tail current amplitudes and fit with single Boltzmann functions. The change in $V_{1/2}$ values ($\Delta V_{1/2}$) observed for $BK_{Ca}$ channel activity upon switching from nominally free to 100 $\mu$M $Ca^{2+}$ at each concentration of cytosolic $Mg^{2+}$ is plotted for the wild-type and E912A/D923A mutant channels (*C*). The observed $\Delta V_{1/2}$ values for the double mutant were found to be significantly different (*, $p < 0.05$) than values for the wild-type channel. For both wild-type and mutant $BK_{Ca}$ channels, recordings from four to seven individual membrane patches were used to calculate the $\Delta V_{1/2}$ values reported under the stated conditions of free cytosolic $Ca^{2+}$ and $Mg^{2+}$.

double mutant in the presence and absence of cytosolic $Ca^{2+}$, under conditions of increasing concentrations of free $Mg^{2+}$ ions. The observed shifts in the G-V relations induced by $Ca^{2+}$ and/or $Mg^{2+}$ in the wild-type channel are qualitatively consistent with those reported earlier (3,33–35,40). Although increasing $Mg^{2+}$ was found to produce a similar shift in the activation of the E912A/D923A mutant channel in the absence of $Ca^{2+}$, little or no shift was evident in the presence of 100 $\mu$M $Ca^{2+}$ (Fig. 6 *B*). Such an effect has not been previously reported for various other $BK_{Ca}$ channel mutations. One possibility that could account for this interesting observation is that the E912A/D923A mutations may reduce the divalent ion binding selectivity of the calcium bowl's high-affinity site, leading to increased displacement of bound $Ca^{2+}$ by $Mg^{2+}$ and a progressive reduction in $Ca^{2+}$-dependent channel activation. In support of this possibility, it has been reported that certain mutations within EF hand motifs are capable of lowering the $Ca^{2+}/Mg^{2+}$ selectivity ratio (13,16,19).

Fig. 6 *C* plots the $Ca^{2+}$-induced $\Delta V_{1/2}$ values observed in the presence of 1, 10, and 80 mM concentrations of cytosolic $Mg^{2+}$. For currents recorded in the presence of 80 mM $Mg^{2+}$, we observed a $\Delta V_{1/2}$ of 153.7 $\pm$ 4.7 mV for the wild-type channel in the presence of 100 $\mu$M $Ca^{2+}$, compared with only 68.5 $\pm$ 1.2 mV for the E912A/D923A double mutant.

Mechanistically, Cui and Aldrich (9) have recently shown that the free-energy contributions provided by membrane voltage ($\Delta G_V$) and the binding of cytosolic free calcium ($\Delta G_{Ca}$) to $BK_{Ca}$ channel activation are additive. As a consequence, the observed leftward shift in G-V relations (i.e., $\Delta V_{1/2}$ value) produced by an increase in the cytosolic [$Ca^{2+}$] should be due primarily to the change in the contribution of calcium binding to the free energy of channel activation (i.e., $\Delta\Delta G_{Ca} = \Delta G_{Ca}$ at low calcium $- \Delta G_{Ca}$ at high calcium). Given that $\Delta G_{Ca} = zeV_{1/2(Ca)}$, it then follows that $\Delta\Delta G_{Ca}$ can be described by the observed calcium-induced leftward shift in the G-V relations, according to the relationship $\Delta\Delta G_{Ca} = (zV_{1/2}$ at low calcium $- zV_{1/2}$ at high calcium$)eN$, where $z =$ the equivalent gating charge derived from fits of the Boltzmann equation to normalized G-V relations for the wild-type and mutant $BK_{Ca}$ channels, $e$ is the elementary charge, and $N$ is Avogadro's number.

Fig. 7 shows a plot of the calculated changes in the free energy of activation due to $Ca^{2+}$ binding after an increase in the cytosolic [$Ca^{2+}$] from ~0 to 100 $\mu$M (e.g., $-\Delta\Delta G_{(5\text{ nM Ca}–100\ \mu\text{M Ca})}$). For the wild-type $BK_{Ca}$ channel, raising the cytosolic [$Mg^{2+}$] from 1 to 10 to 80 mM produced a modest, but insignificant decrease in the calculated change in the free energy of channel opening due to $Ca^{2+}$ binding. Consistent with the findings of Cui, Cox and coworkers (3,33,34), this observation suggests that much of the free-energy change induced by 100 $\mu$M cytosolic $Ca^{2+}$ can be ascribed to binding at the two identified high-affinity sites, as preventing $Ca^{2+}$ binding to the low-affinity site by a large

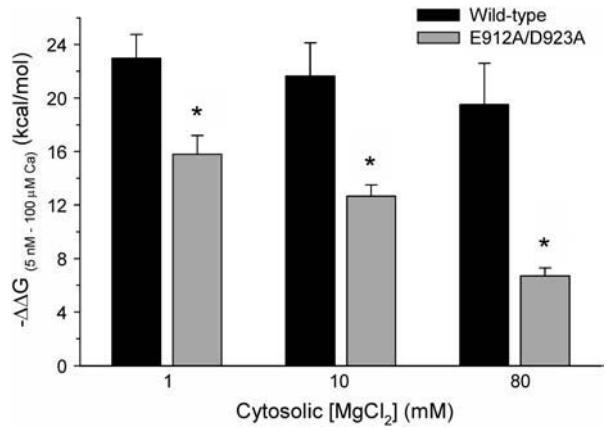


FIGURE 7 Alanine substitution of E912(884) and D923(895) decreases the $Ca^{2+}$-induced change in free energy associated with $BK_{Ca}$ channel activation. Changes in free energy produced by $Ca^{2+}$ binding ($-\Delta\Delta G_{Ca}$) to the high-affinity sites were calculated from differences in the $V_{1/2}$ values of $BK_{Ca}$ channel gating observed in the presence of nominally free and 100 $\mu$M cytosolic $Ca^{2+}$, according to the equation (34): $-\Delta\Delta G_{Ca} = (zV_{1/2,\ 0Ca} - zV_{1/2,\ 100\ \mu M\ Ca})\ eN$, where $e = 1.602 \times 10^{-19}$ C and $N = 6.022 \times 10^{23}$ $mol^{-1}$. Calculations of the $Ca^{2+}$-dependent free-energy changes were carried out at each stated concentration of cytosolic $Mg^{2+}$. For the mutant channels, $-\Delta\Delta G_{Ca}$ values were found to be significantly different than the corresponding values for the wild-type channel (*, $p < 0.05$). Recordings from four to seven individual membrane patches were used to calculate the $-\Delta\Delta G_{Ca}$ values reported at each [$Mg^{2+}$].

excess of $Mg^{2+}$ ions has only very modest effects. However, in the case of our E912A/D923A mutant channel, these same calculated calcium-dependent free-energy changes were found to be significantly less at 1, 10, and 80 mM concentrations of $Mg^{2+}$. Mechanistically, it has been assumed in this analysis that elevated $Mg^{2+}$ acts principally to prevent $Ca^{2+}$-dependent channel activation via the low-affinity divalent ion binding site (i.e., RCK domain), without grossly affecting $Ca^{2+}$ actions via the two high-affinity sites. Although this appears to be largely true in the wild-type channel, the situation may be altered in our E912A/D923A mutant channel, such that high $Mg^{2+}$ may possibly influence the selectivity and/or function of the high-affinity $Ca^{2+}$-binding sites (see above). Recently, Cui and co-workers have reported that elevated $Mg^{2+}$ may interfere with $Ca^{2+}$-dependent channel activation via the high-affinity sites (33) and such effects may account for the modest decline in the calcium-dependent free-energy changes observed in the presence of elevated $Mg^{2+}$ (Fig. 7) (3). If such an effect were enhanced at the level of the calcium bowl in the double mutant channel, then our calculations may in fact overestimate the impact of the E912A/D923A mutations on the free-energy change induced by 100 $\mu$M $Ca^{2+}$.

The data described thus far indicate that the calcium bowl mutations E912(884)A and D923(895)A are able to affect the $Ca^{2+}$-dependent activation of the holo-channel in a synergistic manner. As these residues are predicted to act physically as $Ca^{2+}$-coordinating ligands, based on our homology

model (see Fig. 2 *B*), it may be also anticipated that these same mutations would reduce the direct binding of $Ca^{2+}$ ions to this domain. To examine this prediction experimentally, we first generated cDNA constructs encoding a 148-amino-acid fragment from both the wild-type and mutant $BK_{Ca}$ channels that encompassed the channel's calcium bowl region. These fragments were expressed in bacteria as 6× His fusion proteins and then purified by $Ni^{2+}$ NTA chromatography. Purified proteins were resolved by SDS-PAGE, electrotransferred to nitrocellulose membrane, and then incubated in the presence of radioactive $^{45}Ca$ to examine their $Ca^{2+}$-binding capacity. We (5) and others (2,4) have demonstrated that such fusion proteins are capable of directly binding $^{45}Ca$ using a standard overlay assay.

## Mutations that reduce the calcium sensitivity of $BK_{Ca}$ channel gating also decrease direct $Ca^{2+}$ binding to the calcium bowl domain

Fig. 8 *A* shows a blot of $^{45}Ca$ binding to purified, bacterially expressed protein fragments derived from wild-type and mutant $BK_{Ca}$ channel $\alpha$-subunits. Compared to the wild-type fragment, it is evident that $^{45}Ca$ binding to the fusion proteins derived from the E912(884)A, D923(895)A, and E912A/D923A mutant channels is decreased, whereas binding to the D916(888)A mutant does not appear to be altered. $^{45}Ca$ binding to purified bovine brain calmodulin (CaM), shown in the far left-hand lane, served as a positive control in our experiments. To compare more precisely the levels of $^{45}Ca$ binding, we subsequently stained the purified proteins on the nitrocellulose membrane with amino black (Fig. 8 *B*), and then quantified the actual amount of protein in each lane using image analysis software. The degree of $^{45}Ca$ binding to each full-length, bacterially expressed protein (i.e., ~21 kDa species) was then corrected for the actual amount of protein present on the membrane. For comparison purposes, corrected $^{45}Ca$ binding to each individual mutant protein has been expressed as a percentage of the corrected $^{45}Ca$ binding to the wild-type fragment (Fig. 8 *C*). Based on these analyses, it is evident that the E912(884)A and D923(895)A mutations independently decrease direct $^{45}Ca$ binding to this high-affinity site, whereas combining these two mutations (i.e., E912A/D923A double mutant) produces a synergistic decrease (>50%) in bound $^{45}Ca$.

Fig. 8 *A* also shows the effects of two additional mutations we created within the calcium bowl domain (e.g., DQDDD/NQNNN and ′DKNDE′) on direct $^{45}Ca$ binding. Several independent reports have shown that neutralization/deletion of residues within the Asp-rich sequence of the calcium bowl decreases the apparent calcium sensitivity of $BK_{Ca}$ channel activation (3,25,31). Using a bacterially expressed ~240 amino acid C-terminal fragment from the $BK_{Ca}$ $\alpha$-subunit of *Drosophila melanogastor* (*dSlo*), Bian et al. have reported that neutralization of five Asp residues (i.e., DQDDDDD→DQNNNNN) within the calcium bowl significantly decreased

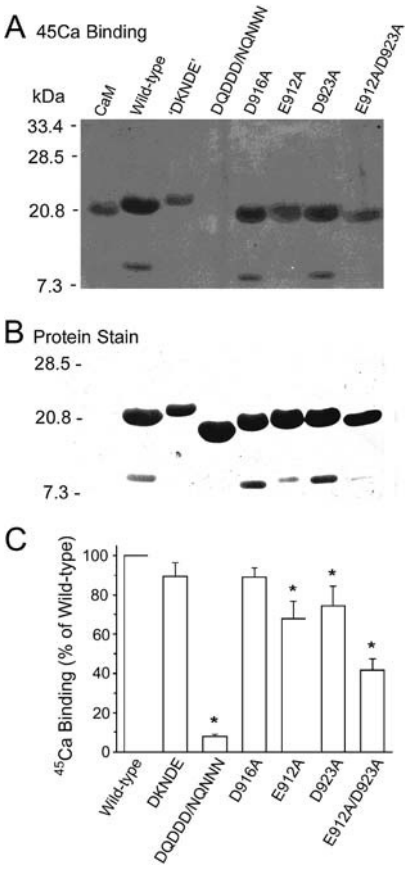


FIGURE 8 Mutations that decrease $Ca^{2+}$-dependent $BK_{Ca}$ channel gating also reduce direct $^{45}Ca$ binding to the calcium bowl domain. A 148-amino-acid fragment ($^{861}$NSPV.. to ..CRVA$^{1009}$) that included the entire C-terminal calcium bowl region was isolated by polymerase chain reaction from the cDNA encoding the wild-type and mutant $BK_{Ca}$ channel $\alpha$-subunits. Individual fragments were expressed as 6× His fusion proteins in bacteria, and similar amounts of purified proteins (15–20 $\mu$g) were then resolved by SDS-PAGE and transferred to nitrocellulose membrane. Panel *A* is an autoradiogram showing $^{45}Ca$ binding to the wild-type and mutant $BK_{Ca}$ channel fusion proteins, along with calmodulin (*CaM*) as a positive control. In addition to the four alanine-substituted channels described in Fig. 2, we examined two additional $BK_{Ca}$ channel mutants, ′DKNDE′ and DQDDD/NQNNN. The modified sequences of these two mutants are described below; amino acid substitutions relative to the wild-type channel have been underlined. Panel *B* shows amido black staining of the nitrocellulose membrane containing the purified wild-type and mutant fusion proteins utilized for $^{45}Ca$ binding in panel *A*. The wild-type protein migrates with a relative molecular weight of ~21 kDa; modest differences in the electrophoretic migration of fusion proteins derived from mutant channels reflect the removal or addition of acidic residues. The lower molecular weight proteins observed in several lanes represent proteolytic fragments of the full-length fusion proteins. In panels *A* and *B*, the positions of molecular weight markers (size in kDa) are indicated by the dashes and numbers on the left-hand side of the panels. (*C*) Direct $^{45}Ca$ binding to individual fusion proteins was quantified using a PhosphorImager (Molecular Dynamics, Piscataway, NJ), and then corrected for the amount of protein detected on the same nitrocellulose membrane by amido black staining. $^{45}Ca$ binding to mutant proteins is expressed relative to wild-type binding (100%); values represent the means ± SE derived from three individual experiments. Wild-type sequence, ELVNDTNVQFLDQDDD; DKNDE mutant, DKNNDTNVDFLEQDDD; DQDDD/NQNNN mutant, ELVNDTNVQFLNQNNN.

direct $^{45}Ca$ binding to this fragment, but did not have a major effect on the activation of the channel by cytosolic $Ca^{2+}$ (4). More recently, Bao and colleagues have reported that alanine substitution of acidic residues within the calcium bowl region (i.e., DQDDDDD → DQDADDD or DQDDDAD) has significant effects on both $Ca^{2+}$-dependent channel activation and $^{45}Ca$ binding to a bacterially expressed GST-fusion protein encompassing this region (2). G-V curves for the DQDDD/NQNNN mutant channel displayed much smaller leftward shifts at 1 and 10 $\mu$M calcium compared to the wild-type channel (data not shown), and appeared similar to the G-V curves described for the 5D/5N mutant channel (31,38). Our observation that the DQDDD/NQNNN series of mutations strongly inhibited direct $^{45}Ca$ binding is also in agreement with the inhibitory effects observed by Bao and colleagues after alanine replacement of residues within this sequence (2).

Authentic EF hands display considerable variation in their primary sequences (13,23), and this variability may account for observed differences in their $Ca^{2+}$-binding affinities (i.e., $K_D$ values), which may range from 0.1 to 1 $\mu$M. We thus postulated that it may be possible to ''improve'' the $Ca^{2+}$-binding properties of the calcium bowl by substituting amino acids found more typically within EF hand motifs. For example, in the $\beta$-isoform of parvalbumin, replacing neutral residues at the +Z and −Y positions within the EF hand loop sequence by aspartic acids was observed to enhance the $Ca^{2+}$-binding affinity of the mutant protein (16). Based on such findings, we constructed the ′DKNDE′ $BK_{Ca}$ channel mutant (described in the legend for Fig. 8) by replacing amino acids in key positions with those found in calmodulin (i.e., refer to EF hand sequence displayed in Fig. 1). In contrast to the results reported for parvalbumin, the ′DKNDE′ mutant channel did not display greater $^{45}Ca$ binding compared with the fusion protein derived from the wild-type channel (Fig. 8 *C*). Similarly, we observed that a mutant $BK_{Ca}$ channel containing the ′DKNDE′ series of substitutions did not display enhanced activation in the presence of either 1 or 10 $\mu$M free $Ca^{2+}$ (data not shown).

Collectively, the data described in our study provide a number of additional insights regarding the contribution of calcium bowl residues to the $Ca^{2+}$ dependence of $BK_{Ca}$ channel activation. Specifically, we have: 1), firmly identified the contributions of E912(884) and D923(895) to calcium bowl function by using a broad range of free $Ca^{2+}$ concentrations to reveal the effects of these individual point mutations on channel activation; 2), demonstrated that mutations decreasing the $Ca^{2+}$ sensitivity of channel gating also reduce the time constants of channel activation/deactivation, as would be predicted from the noted $Ca^{2+}$ dependence of current kinetics; 3), observed that the E912(884)A and D923(895)A mutations act in a synergistic manner to decrease both the $Ca^{2+}$ sensitivity of $BK_{Ca}$ channel gating and direct $^{45}Ca$ binding to the calcium bowl domain, which is consistent with the behavior of multivalent $Ca^{2+}$ ion binding sites; and 4), described a novel change in the activation of the E912A/D923A double mutant channel in the presence of $Ca^{2+}$ and elevated $Mg^{2+}$, which may reflect an interesting effect of these mutations to influence the action of $Mg^{2+}$ ions on the channel's high-affinity $Ca^{2+}$-binding sites.

## DISCUSSION

Over the past several years, considerable evidence has highlighted the contribution of the C-terminal calcium bowl domain to the $Ca^{2+}$ sensitivity of $BK_{Ca}$ channel gating (22). Despite the recognized functional importance of this region, little is known about its underlying structural features, in particular, those that may contribute to its putative high-affinity $Ca^{2+}$-binding site. Several studies have clearly demonstrated that a series of five Asp residues is critically involved in the function of this domain (2,4,31,32,38), however, it remains unclear exactly how these acidic amino acids contribute to $Ca^{2+}$-dependent channel activation and $Ca^{2+}$ ion binding. In an earlier study (5), we had suggested that an amino acid sequence within the calcium bowl may resemble an EF hand motif, based on the positions of potential $Ca^{2+}$-coordinating ligands (i.e., residues with oxygen-containing side chains) and the similarity of residues to those existing within authentic EF hand structures (13,23). In this study, we have pursued this possibility by employing a homology modeling strategy to generate a predicted structure of this region, using the atomic coordinates of a $Ca^{2+}$-bound EF hand from human calmodulin as a structural template (see Fig. 2). As anticipated, the resulting three-dimensional model reveals individual acidic residues in this region of the $BK_{Ca}$ $\alpha$-subunit that may potentially act as $Ca^{2+}$-coordinating ligands, based on the spatial orientation of oxygen atoms in their side-chain groups. To evaluate the predictions arising from this model, we have utilized a multifaceted strategy involving site-directed mutagenesis, electrophysiologic measurements of $Ca^{2+}$-dependent channel activation and the binding of radioactive $^{45}Ca$ to the calcium bowl expressed as a bacterial fusion protein.

### Evaluation of model predictions and experimental data

Electrophysiological recordings of wild-type and mutant $BK_{Ca}$ channels in excised membrane patches of HEK 293 cells revealed that the individual E912(884)A and D923(895)A mutations decreased the $Ca^{2+}$ sensitivity of steady-state $BK_{Ca}$ channel gating, as judged by the magnitude of $Ca^{2+}$-induced leftward shifts in the individual G-V curves (Figs. 3 and 4). In contrast, mutant channels bearing either N918(890)A or Q920(892)A substitutions did not display changes in their $Ca^{2+}$ sensitivity under the same recording conditions. Although we could not evaluate the N915(887)A mutant, due to poor expression, it was recently reported that this same mutation did not affect the $Ca^{2+}$ sensitivity of another murine $BK_{Ca}$ channel clone expressed in *Xenopus*

oocytes (2). Taken together, these results suggest that the side chains of residues N915(887), N918(890), and Q920(892) do not contribute to the functional $Ca^{2+}$ sensitivity of $BK_{Ca}$ channel activation via the calcium bowl domain. Such observations may reflect both the lack of net charge of these side-chain groups and their predicted orientation away from the bound $Ca^{2+}$ ion in our model (Fig. 2 *B*).

Several of the above findings agree closely with the recent results of Bao and colleagues, who utilized alanine scanning mutagenesis to ''map'' functionally important residues within the calcium bowl region (2). In their study, they noted the reduced $Ca^{2+}$-dependent activation of the D923(895)A mutant, which we had originally described (5), and the lack of effect of alanine substitutions at residues N918(890) and Q920(892). However, our results further indicate that E912(884) influences the $Ca^{2+}$ sensitivity of $BK_{Ca}$ channel activation at cytosolic [$Ca^{2+}$]s below 10 $\mu$M (refer to Fig. 4); as Bao and colleagues only examined this mutant in the presence of 0 and 10 $\mu$M cytosolic $Ca^{2+}$, it is unlikely that the contribution of E912(884) toward $Ca^{2+}$-dependent channel activation would have been detected under their experimental conditions.

Combining the E912(884)A and D923(895)A mutations produced a more noticeable reduction in the $Ca^{2+}$-dependent changes in $V_{1/2}$ values, as well as a slowing of macroscopic current activation and an acceleration of current deactivation (Figs. 3 and 5). As the $Ca^{2+}$ dependence of both these kinetic effects is well recognized (10,12), the altered activity of the E912A/D923A double mutant appears to be consistent with a functional decrease in the channel's $Ca^{2+}$ responsiveness. Structural studies have revealed that the selective coordination of single $Ca^{2+}$ ions within both proteins and organic calcium chelators, such as EGTA, occurs via multiple oxygen atoms that are arranged to form rigid binding pockets or cavities (13). One could thus postulate that a combination of mutations, such as E912A/D923A or replacement of the Asp-rich region in the calcium bowl (i.e., 5D5N), leads to a greater decrease in the $Ca^{2+}$ sensitivity of $BK_{Ca}$ channel gating, as a result of these mutations on a multivalent binding site. Although Bao and colleagues noted that the $Ca^{2+}$ sensitivity of $BK_{Ca}$ channel gating/energetics was strongly reduced by several of their mutations (e.g., D898A and D900A), the functional consequences of combining such mutations on $Ca^{2+}$-dependent channel gating over a broad range of $Ca^{2+}$ concentrations, as well as the kinetics of current activation/deactivation, were not examined.

Using an independent assay, we further observed that the E912(884)A and D923(895)A mutations decreased the amount of radioactive calcium ($^{45}Ca$) directly bound to a 148-amino-acid fragment of the $BK_{Ca}$ channel's C-terminus containing the calcium bowl domain expressed as a bacterial fusion protein (see Fig. 8). Consistent with our electrophysiological data, the E912A/D923A double mutation decreased $^{45}Ca$ binding more than either substitution alone. In their study, Bao and colleagues reported that E912(884)A produced a modest, but insignificant decrease in $^{45}Ca$ binding to their bacterially expressed, calcium bowl fusion protein, but they did not examine $^{45}Ca$ binding to the D923(895)A mutant. Similar to our findings, this group also observed that combining mutations that individually reduced the channel's functional $Ca^{2+}$ sensitivity (e.g., D926(898) and D928(900)) resulted in a larger decrease in $^{45}Ca$ binding compared to either mutation alone.

In a canonical EF hand, as found in calmodulin or troponin C, residue D923(895) would function as a bidentate $Ca^{2+}$-binding ligand, occupying the $-Z$ position in the $Ca^{2+}$ ion coordination loop. In our model, the side chain of D923(895) is correctly oriented to participate in $Ca^{2+}$ binding, and replacement of this single residue was observed to reduce the channel's apparent $Ca^{2+}$ sensitivity. Alanine substitution of E912(884), which would occupy the X position within an EF hand binding loop, was also found to reduce $Ca^{2+}$-dependent channel activation, but in this case, the effect occurred primarily at low concentrations (e.g., $<10$ $\mu$M) of cytosolic $Ca^{2+}$. In calmodulin and troponin C, replacement of the acidic residue in this X position decreases both $Ca^{2+}$ binding and protein function (14,28). In contrast to the predictions of our model, alanine replacement of D916(888) did not alter either the channel's apparent $Ca^{2+}$ sensitivity, or direct $^{45}Ca$ binding to a bacterial fusion protein containing this same mutation (Figs. 4 and 8).

## Parallels between calcium-sensitive $BK_{Ca}$ channel gating and EF hands

Two properties of EF hands that may be of particular relevance to the $Ca^{2+}$ sensitivity of $BK_{Ca}$ channel gating are: 1), the selectivity of their metal ion binding sites, and 2), their ability to undergo state-dependent changes in $Ca^{2+}$-binding affinity. EF hands are known to bind divalent cations with exquisite selectivity, displaying a typical activation sequence of $Ca^{2+} > Sr^{2+} \gg Cd^{2+}$, $Mg^{2+}$, $Ba^{2+}$ (13). Using a series of mutations capable of disabling each of the $BK_{Ca}$ channel's putative high- and low-affinity cation binding sites, Lingle and co-workers (39) have now demonstrated that these three sites can be functionally distinguished based on their selective activation by a series of divalent cations. In particular, it was observed that channel activation via the calcium bowl-associated high-affinity site could be mediated by low concentrations (e.g., 10 $\mu$M) of either $Ca^{2+}$ or $Sr^{2+}$, but not other divalent metals with smaller atomic radii, such as $Mn^{2+}$, $Cd^{2+}$, $Co^{2+}$, or $Ni^{2+}$. It is noteworthy that this activation profile of the calcium bowl domain appears to mirror the divalent cation selectivity displayed by a number of EF hand structures. These same investigators also reported that channel activation via the second high-affinity site (D362/D367), located within the channel's RCK domain (17), could be effectively mediated by $Cd^{2+}$, along with $Ca^{2+}$ and $Sr^{2+}$. Accommodation of a smaller $Cd^{2+}$ ion may

suggest that this second site differs in its metal ion coordination geometry compared to the calcium bowl site (13).

Extensive kinetic analyses have indicated that the $Ca^{2+}$-dependent activation of $BK_{Ca}$ channels can be readily explained by an allosteric gating mechanism (22), in which the open state of the channel necessarily displays a higher $Ca^{2+}$ ion binding affinity than that of the closed state. In this context, it may be revealing that EF hand-containing proteins (e.g., calmodulin) also undergo conformation-dependent increases in $Ca^{2+}$-binding affinity that typically occur in the presence of a cognate target protein (13). In the holo-$BK_{Ca}$ channel, structural rearrangements associated with transition to the open state, or those leading to interaction with another domain, may be sufficient to initiate such an affinity change within a putative EF hand-like binding site. This ability of EF hands to undergo a state-dependent change in their divalent cation binding affinity thus appears to be consistent with a key molecular aspect of the allosteric gating mechanism described for $BK_{Ca}$ channels (3,8,29).

## An EF hand structural model in relation to other calcium bowl mutations

It may be reasonable to expect that any structural model suggested to underlie the putative high-affinity $Ca^{2+}$ ion binding site in the calcium bowl domain should also encompass data describing the loss of functional $Ca^{2+}$ sensitivity and direct $^{45}Ca$ binding after neutralization of negative charges in the calcium bowl domain, as we (see Fig. 8) and others have demonstrated (2,4). In this context, earlier studies have shown that $Ca^{2+}$ binding within an EF hand structure can be strongly influenced by neighboring protein surface charges present within the same domain. In the case of the two EF hands of calbindin $D_{9K}$, neutralizing up to three acidic residues positioned near the two identified $Ca^{2+}$-binding sites dramatically decreased $Ca^{2+}$ affinity, even though the side chains of these residues did not directly act as coordinating ligands (18,20). Rather, these negatively charged residues appear to influence $Ca^{2+}$ binding via long-range electrostatic effects, based on their proximity (8–12 Å) to the bound $Ca^{2+}$ ions. Similarly, it is conceivable that the Asp-rich sequence in the calcium bowl exerts a similar influence, both within the holo-channel and in bacterially expressed fusion proteins. In our model, the side chains of the first four residues in this region (i.e., from D925(897) to D928(900)) are predicted to lie within 10.5 Å of the bound $Ca^{2+}$ ion (see Fig. 2 *B*). If one postulated that the actual high-affinity $Ca^{2+}$-binding site within the calcium bowl domain consisted of a weak EF hand containing a suboptimal number of coordinating oxygen atoms, then this series of acidic residues would be expected to take on an increased functional importance in maintaining the integrity of the binding site, as a result of their electrostatic influence. However, it is also apparent that this same Asp-rich region does not function simply as a cluster of negative charges, as both the length of these charged side chains, as well as their positions within the series, influence the $Ca^{2+}$ sensitivity of channel gating and direct $^{45}Ca$ binding to the calcium bowl (2). For example, replacement of D926(898) or D928(900) by Glu disrupts both $Ca^{2+}$ sensitivity and $^{45}Ca$ binding, whereas alanine substitution of D927(899) does not affect $Ca^{2+}$-dependent activation, but does reduce $^{45}Ca$ binding. In the holo-channel, D927(899) may be neutralized by pairing with a positively charged side chain, whereas in a bacterial fusion protein, such interactions may be lost. In the case of D926(898) and D928(900), increasing side-chain length may disrupt local conformation within the calcium bowl, leading to decreased $Ca^{2+}$ binding in both the holo-channel and fusion protein. Alternatively, it is equally conceivable that these aspartic acids act as direct $Ca^{2+}$-binding ligands, as Bao and colleagues have suggested (2).

In other membrane channels, EF hand motifs have been implicated in the $Ca^{2+}$ sensitivity of twin-pore $K^+$ channels (11,30) and cardiac sodium channels (37), and the possibility exists that a similar mechanism of $Ca^{2+}$ sensitivity may be conserved in $BK_{Ca}$ channels. However, not all noted EF hand sequences may function in this manner. For example, in voltage-gated L, N, and P/Q-type calcium channels, a C-terminal EF hand motif appears to serve as a ''transduction module'' that participates in $Ca^{2+}$-induced inactivation via a calmodulin subunit constitutively bound to the channel's pore-forming $\alpha$-subunit (27).

## Can we conclude that the calcium bowl region functions as a $Ca^{2+}$ sensor?

Although we favor the possibility that neutralization of negative charges at positions E912(884) and D923(895), as well as neighboring aspartic acids (2,4), lowers the channel's $Ca^{2+}$ sensitivity by directly interfering with $Ca^{2+}$ binding within the calcium bowl, it is equally possible that these mutations in the holo-channel act through other molecular mechanisms. As discussed by Cox and colleagues (2), mutations that disrupt the $Ca^{2+}$ sensitivity of $BK_{Ca}$ channel opening may affect the difference in $Ca^{2+}$ affinities described for the closed and open states of the channel (3,9,29) or may allosterically reduce either direct $Ca^{2+}$ ion binding or the transduction of $Ca^{2+}$-binding energy from a distinct site physically beyond the calcium bowl to the gating machinery in the channel core, as a result of structural rearrangement within the calcium bowl domain. Thus, it appears that atomically resolved structures of the $BK_{Ca}$ channel's C-terminus in both the apo- and $Ca^{2+}$-bound states will be ultimately needed to identify the structural elements underlying this putative high-affinity binding site and how they contribute to the $Ca^{2+}$ sensitivity of $BK_{Ca}$ channel gating.

This work was supported by Canadian Institutes of Health Research operating grants to A. P. Braun and H. J. Vogel, and an Alberta Heritage Foundation for Medical Research establishment grant (to A.P.B.). A. P. Braun gratefully acknowledges a senior research scholarship from the Alberta Heritage Foundation for Medical Research.

## REFERENCES


1. Adelman, J. P., K.-Z. Shen, M. P. Kavanaugh, R. A. Warren, Y.-N. Wu, A. Lagrutta, C. T. Bond, and R. A. North. 1992. Calcium-activated potassium channels expressed from cloned complementary DNAs. *Neuron*. 9:209–216.
2. Bao, L., C. Kaldany, E. C. Holmstrand, and D. H. Cox. 2004. Mapping the $BK_{Ca}$ channel's 'calcium bowl': side-chains essential for $Ca^{2+}$ sensing. *J. Gen. Physiol.* 123:475–489.
3. Bao, L., A. M. Raoin, E. C. Holmstrand, and D. H. Cox. 2002. Elimination of the $BK_{Ca}$ channel's high-affinity $Ca^{2+}$ sensitivity. *J. Gen. Physiol.* 120:173–189.
4. Bian, S., I. Favre, and E. Moczydlowski. 2001. $Ca^{2+}$-binding activity of a COOH-terminal fragment of the *Drosophila* BK channel involved in $Ca^{2+}$-dependent activation. *Proc. Natl. Acad. Sci. USA*. 98:4776–4781.
5. Braun, A. P., and L. Sy. 2001. Contribution of potential EF hand motifs to the calcium-dependent gating of a mouse brain large conductance, calcium-sensitive $K^+$ channel. *J. Physiol. (Lond.)*. 533:681–695.
6. Bulter, A., S. Tsunoda, D. P. McCobb, A. Wei, and L. Salkoff. 1993. *mSlo*, a complex mouse gene encoding 'maxi' calcium-activated potassium channels. *Science*. 261:221–224.
7. Chattopadhyaya, R., W. E. Meador, A. R. Means, and F. A. Quiocho. 1992. Calmodulin structure refined at 1.7 Å resolution. *J. Mol. Biol.* 228:1177–1192.
8. Cox, D. H., and R. W. Aldrich. 2000. Role of the $\beta$1 subunit in large conductance $Ca^{2+}$-activated $K^+$ channel gating energetics. Mechanisms of enhanced $Ca^{2+}$ sensitivity. *J. Gen. Physiol.* 116:411–432.
9. Cui, J., and R. W. Aldrich. 2000. Allosteric linkage between voltage and $Ca^{2+}$-dependent activation of BK-type mSlo1 $K^+$ channels. *Biochemistry*. 39:15612–15619.
10. Cui, J., D. H. Cox, and R. W. Aldrich. 1997. Intrinsic voltage dependence and $Ca^{2+}$ regulation of *mSlo* large conductance Ca-activated $K^+$ channels. *J. Gen. Physiol.* 109:647–673.
11. Czempinski, K., S. Zimmermann, T. Ehrhardt, and B. Müller-Röber. 1997. New structure and function in plant $K^+$ channels: KCO1, an outward rectifier with a steep $Ca^{2+}$ dependency. *EMBO J.* 16:2565–2575.
12. DiChiara, T. J., and P. H. Reinhart. 1995. Distinct effects of $Ca^{2+}$ and voltage on the activation and deactivation of cloned $Ca^{2+}$-activated $K^+$ channels. *J. Physiol. (Lond.)*. 489:403–418.
13. Falke, J. J., S. K. Drake, A. L. Hazard, and O. B. Peersen. 1994. Molecular tuning of ion binding to calcium signaling proteins. *Q. Rev. Biophys.* 27:219–290.
14. Geiser, J. R., D. van Tuinen, S. E. Brockerhoff, M. M. Neff, and T. N. Davis. 1991. Can calmodulin function without binding calcium? *Cell*. 65:949–959.
15. Ha, T. S., S. Y. Jeong, S.-W. Cho, H.-K. Jeon, G. S. Roh, W. S. Choi, and C.-S. Park. 2000. Functional characteristics of two $BK_{Ca}$ channel variants differentially expressed in rat brain tissues. *Eur. J. Biochem.* 267:910–918.
16. Henzl, M. T., R. C. Hapak, and E. A. Goodpasture. 1996. Introduction of a fifth carboxylate ligand heightens the affinity of the oncomodulin CD and EF sites for $Ca^{2+}$. *Biochemistry*. 35:5856–5869.
17. Jiang, Y., A. Pico, M. Cadene, B. T. Chait, and R. MacKinnon. 2001. Structure of the RCK domain from the *E. coli* $K^+$ channel and demonstration of its presence in the human BK channel. *Neuron*. 29:593–601.
18. Linse, S., P. Brodin, C. Johansson, E. Thulin, T. Grundström, and S. Forsén. 1988. The role of protein surface charges in ion binding. *Nature*. 335:651–652.
19. Linse, S., and S. Forsén. 1995. Determinants that govern high-affinity calcium binding. *In* Advances in Second Messenger and Phosphoprotein Research. A. R. Means, editor. Raven Press, New York, NY. 89–151.
20. Linse, S., C. Johansson, P. Brodin, T. Grundström, T. Drakenberg, and S. Forsén. 1991. Electrostatic contributions to the binding of $Ca^{2+}$ in calbindin $D_{9K}$. *Biochemistry*. 30:154–162.
21. Lippiat, J. D., N. B. Standen, and N. W. Davies. 1998. Block of cloned $BK_{Ca}$ channels (*rSlo*) expressed in HEK 293 cells by N-methyl D-glucamine. *Pflugers Arch.* 436:810–812.
22. Magleby, K. L. 2003. Gating mechanism of BK (Slo1) channels: so near, yet so far. *J. Gen. Physiol.* 121:81–96.
23. Marsden, B. J., G. S. Shaw, and B. D. Sykes. 1990. Calcium binding proteins. Elucidating the contributions to calcium affinity from an analysis of species variants and peptide fragments. *Biochem. Cell Biol.* 68:587–601.
24. Moncrief, N. D., R. H. Kretsinger, and M. Goodman. 1990. Evolution of EF-hand calcium-modulated proteins. I. Relationships based on amino acid sequences. *J. Mol. Evol.* 30:522–562.
25. Nui, X., and K. L. Magleby. 2002. Stepwise contribution of each subunit to the cooperative activation of BK channels by $Ca^{2+}$. *Proc. Natl. Acad. Sci. USA*. 99:11441–11446.
26. Pallanck, L., and B. Ganetzky. 1994. Cloning and characterization of human and mouse homologs of the *Drosophilia* calcium-activated potassium channel gene, *slowpoke*. *Hum. Mol. Genet.* 3:1239–1243.
27. Peterson, B. Z., J. S. Lee, J. G. Mulle, Y. Wang, M. de Leon, and D. T. Yue. 2000. Critical determinants of $Ca^{2+}$-dependent inactivation within an EF-hand motif of L-type $Ca^{2+}$ channels. *Biophys. J.* 78: 1906–1920.
28. Putkey, J. A., H. L. Sweeney, and S. T. Campbell. 1989. Site-directed mutagenesis of the trigger calcium-binding sites in cardiac troponin C. *J. Biol. Chem.* 264:12370–12378.
29. Rothberg, B. S., and K. L. Magleby. 2000. Voltage and $Ca^{2+}$ activation of single large-conductance $Ca^{2+}$-activated $K^+$ channels described by a two-tiered allosteric gating mechanism. *J. Gen. Physiol.* 116:75–99.
30. Salinas, M., R. Reyes, F. Lesage, M. Fosset, C. Heurteaux, G. Romey, and M. Lazdunski. 1999. Cloning of a new mouse two-P domain channel subunit and a human homologue with a unique pore structure. *J. Biol. Chem.* 274:11751–11760.
31. Schreiber, M., and L. Salkoff. 1997. A novel calcium-sensing domain in the BK channel. *Biophys. J.* 73:1355–1363.
32. Schreiber, M., A. Yuan, and L. Salkoff. 1999. Transplantable sites confer calcium sensitivity to BK channels. *Nat. Neurosci.* 2:416–421.
33. Shi, J., and J. Cui. 2001. Intracellular $Mg^{2+}$ enhances the function of BK-type $Ca^{2+}$-activated $K^+$ channels. *J. Gen. Physiol.* 118:589–605.
34. Shi, J., G. Krishnamoorthy, Y. Yang, L. Hu, N. Chaturvedi, D. Harilal, and J. Cui. 2002. Mechanism of magnesium activation of calcium-activated potassium channels. *Nature*. 418:876–880.
35. Wei, A., C. Solaro, C. Lingle, and L. Salkoff. 1994. Calcium sensitivity of BK-type $K_{Ca}$ channels determined by a separable domain. *Neuron*. 13:671–681.
36. Weljie, A. M., T. E. Clarke, A. H. Juffer, A. C. Harmon, and H. J. Vogel. 2000. Comparative modeling studies of the calmodulin-like domain of calcium-dependent protein kinase from soybean. *Proteins*. 39:343–357.
37. Wingo, T. L., V. N. Shah, M. E. Anderson, T. P. Lybrand, J. W. Chazin, and J. R. Balser. 2004. An EF-hand in the sodium channel couples intracellular calcium to cardiac excitability. *Nat. Struct. Mol. Biol.* 11:219–225.
38. Xia, X.-M., X. Zeng, and C. J. Lingle. 2002. Multiple regulatory sites in large-conductance calcium-activated potassium channels. *Nature*. 418:880–884.
39. Zeng, X.-H., X.-M. Xia, and C. Lingle. 2005. Divalent cation sensitivity of BK channel activation supports the existence of three distinct binding sites. *J. Gen. Physiol.* 125:273–286.
40. Zhang, X., C. R. Solaro, and C. J. Lingle. 2001. Allosteric regulation of BK channel gating by $Ca^{2+}$ and $Mg^{2+}$ through a nonselective, low affinity divalent cation site. *J. Gen. Physiol.* 118:607–635.